Chemistry Africa (2025) 8:2271–2284
https://doi.org/10.1007/s42250-025-01274-4

ORIGINAL ARTICLE

Customizing Indolin-2-One-Thiosemicarbazones: Design, Synthesis, Anti-proliferative Assessment Along with In Silico and Electrochemical Investigations

Preeti[1] · Bharvi Sharma[1] · Sarbjeet Kaur[1] · Shanen Perumal[2] · Gabriella Palma[2] · Mandeep Kaur[2] · Inderpreet Kaur[1] · Vipan Kumar[1]

Received: 9 January 2025 / Accepted: 17 March 2025 / Published online: 15 April 2025

Abstract
In this study, we report the design, synthesis, and anti-proliferative effects of 1*H*-1,2,3-triazole-linked indolin-2-one-bis(thiosemicarbazone/semicarbazones) against estrogen-responsive (MCF-7) and triple-negative (MDA-MB-231) breast cancer cells. Notably, compound **6b**, featuring F-substitution at the C-5 position of indole and thiosemicarbazone, exhibited a notable IC_{50} value of 71.65 µM against MCF-7 cells and displayed non-cytotoxicity towards normal kidney cells. To unravel its potential mechanism of action, molecular docking and electrochemical studies were conducted. Electrochemical analysis revealed the compound's ability to chelate Fe(III), a component present in the active site of ribonucleotide reductase. Furthermore, **6b** displayed significant binding affinity at the active site of ribonucleotide reductase, as indicated by molecular docking. These collective findings suggest that compound **6b** holds promise as a potential inhibitor of ribonucleotide reductase.

Keywords Antiproliferative · Fe(III) chelation · Indolin-2-one-thiosemicarbazones · In silico · Ribonucleotide reductase inhibition · 1,2,3-triazole

1 Introduction

Cancer stands as a critical healthcare issue globally, with breast cancer being a significant contributor, primarily affecting women. The US was projected to have 43,170 cancer fatalities and 300,590 new cancer cases in 2023, according to the American Cancer Society [1]. Breast cancer, though less common, can also afflict men, accounting for about 0.5–1% of all cases [2]. Most of the breast cancer cases involve women aged 40 and older, who are at a heightened risk [3]. Multiple factors contribute to the risk of developing breast cancer, including smoking, exposure to radiation, aging, obesity, excessive alcohol consumption, reproductive history (such as the age at first menstrual period and age at first pregnancy), and postmenopausal hormone therapy [4, 5]. In high-income countries, the survival rate for breast cancer exceeds 90% over a five-year period, whereas it is 66% in India and 40% in South Africa [6]. Tamoxifen is a 'Gold standard' of hormonal therapy, but its use is limited by: (i) emergence of tumor resistance; (ii) severe side effects, including chances of endometrial cancer; and (iii) high frequency of disease relapse (40% BC cases receiving Tamoxifen therapy eventually encounter relapse) [7].

Schiff bases are known to be of great importance in the field of medicinal chemistry. The semi-or thiosemicarbazones have the ability to block the enzyme ribonucleotide reductase, which is necessary for DNA synthesis, or they can selectively chelate with physiologically important trace metal ions. Both of these processes are likely to account for their anticancer properties [8]. Among these derivatives, Triapine (**I**) emerges as the most promising therapeutic compound, standing out as a significantly more potent RNR inhibitor compared to hydroxyurea (HU). Triapine's potency is ~ 1000 times greater than that of HU, making it a notable candidate for inclusion in several phase II clinical trials as a potential chemotherapeutic agent [9]. Unfortunately,

Preeti and Bharvi Sharma contributed equally to this work.

✉ Vipan Kumar
vipan_org@yahoo.com

[1] Department of Chemistry, Guru Nanak Dev University, Amritsar 143005, India

[2] School of Molecular and Cell Biology, University of the Witwatersrand, Private Bag 3, Wits-2050, Johannesburg, South Africa

its clinical use is hampered by severe side effects [10]. In addition to Triapine, other thiosemicarbazone-based drug candidates, such as di-2-pyridylketone 4-cyclohexyl-4-methyl-3-thiosemicarbazone (DpC) (**II**)and COTI-2 (**III**), are currently undergoing Phase I clinical trials for gynecologic malignancies and resistant solid tumors, respectively [11, 12]. Few examples of semicarbazone based anticancer drugs include Parthenolide-derived semicarbazone (**IV**) and Vanillin semicarbazone (VSC) (**V**) [13, 14].

Isatin serves as a promising scaffold with considerable potential in a wide range of biological activities. It is found in variety of plants such as *Isatis tinctoria*, *Couroupita guianensis Aubl*, *Melochia tomentosa*, and *Boronia koniamboensis*. It is also found in the parotid glands of Australian mollusc *Dicathais orbita* and Bufo frogs. It exists in bodily fluids, peripheral tissues, and the central nervous system of humans and is identified as a tryptophan or epinephrine metabolite. Owing to its unique molecular structure, isatin provides a flexible platform for structural modification and derivatization. It can act as both nucleophile as well as an electrophile. Isatin-based compounds have shown good tolerance in humans, and several derivatives are currently on the market, clinically utilized for the treatment of various cancers. Notable examples include sunitinib (**VI**), Semaxanib (**VII**), and orantinib (**VIII**) [15–18]. Additionally, isatin exhibits a broad spectrum of biological activities, including antibacterial, antifungal, antitubercular, antidiabetic, neuroprotective, anticonvulsant, anti-HIV, analgesic, antioxidant, anti-inflammatory, anti-glycation, antimalarial, and anti-anxiety properties [19–23]. Based on this rationale, we designed a library of Indolin-2-one-thiosemicarbazones conjugates (Fig. 1).

Recent findings from our laboratory have highlighted the anti-proliferative potential of molecular hybrids based on isatin [24–26]. In the current study, we have extended this research to involve the synthesis and evaluation of the anti-proliferative effects of 1*H*-1,2,3-triazole-linked indolin-2-one-bis(thiosemicarbazone/semicarbazones) on MCF-7 (estrogen-responsive/ER+) and MDA-MB-231 (triple-negative/ER−) cells. Additionally, we conducted *in-silico* studies and followed up with comprehensive spectroscopic and electrochemical investigations to elucidate the mode of action of these compounds.

2 Results and Discussion

2.1 Synthetic Chemistry

The first step involved the base promoted propargylation of C-5/C-7 substituted isatins **1** resulted in formation of *N*-propargylated isatins **2** which were then subjected to Cu promoted click reactions with *O*-azidobenzaldehyde **4** to yield precursors, **5a–f** (Scheme 1).

Further, treatment of precursor **5a–f** with thiosemicarbazide/semicarbazide in ethanol and a catalytic amount of glacial acetic acid afforded the corresponding compounds **6a–f** and **7a–f** (Scheme 2) [27]. The structure of the target compounds was assigned based on analytical evidences and spectral data. For example, compound **6b** exhibited molecular ion peak at $[M+H]^+$ 497.1189 in its High Resolution Mass Spectrum (HRMS). Its ^{1}H NMR exhibited characteristic singlets at δ 5.16, 8.01, and 8.29 corresponding to methylene, triazole ring and iminic protons. The presence of distinctive absorptions at δ 35.1, 160.5, 178.6, and 179.2, corresponding to methylene, the cyclic amide (–NC(O)) of isoindoline, ketimine (C=N), and amide carbons of

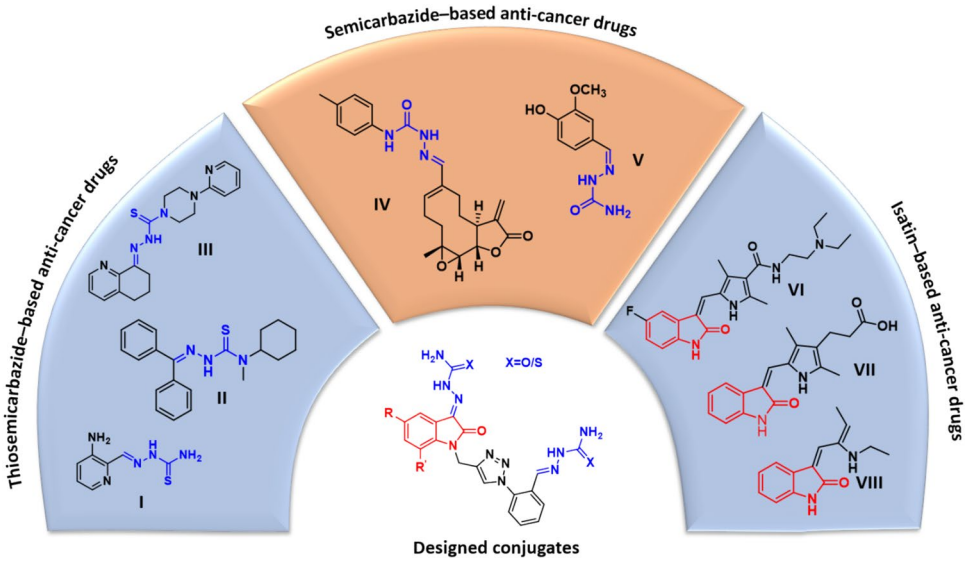

Fig. 1 Schematic diagram depicting design strategy for choosing the molecular fragments (highlighted) in the synthesis of Indolin-2-one-thiosemicarbazones conjugates

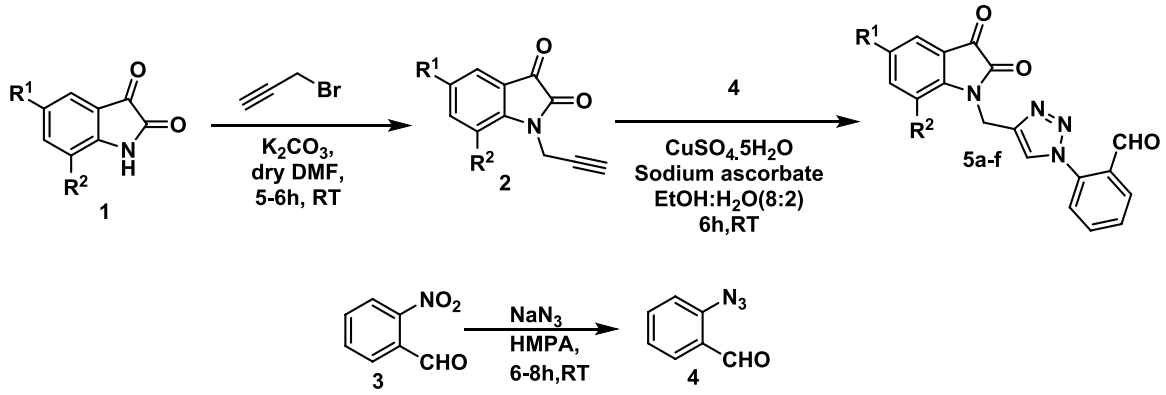

Scheme 1 Synthesis of precursors **5a–f**

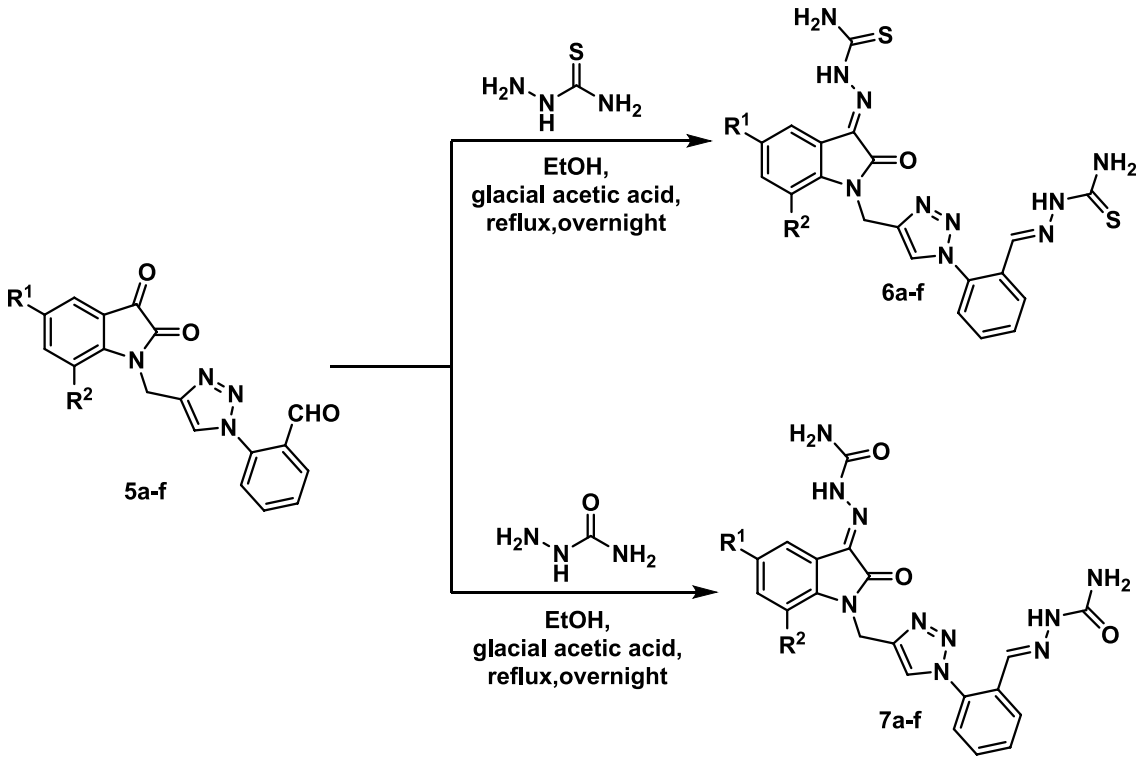

Entry	R^1	R^2
5a/6a/7a	H	H
5b/6b/7b	F	H
5c/6c/7c	Cl	H
5d/6d/7d	OMe	H
5e/6e/7e	Br	H
5f/6f/7f	Br	Br

Scheme 2 Synthesis of isoindolin-2-one-thiosemicarbazone **6a–f** and isoindolin-2-one-semicarbazone **7a–f**

thiosemicarbazone in the ^{13}C NMR spectrum, further supported the assigned structure.

2.2 In Vitro Anti-proliferative Assessment

The anti-proliferative activities of synthesized compounds **5a–f**, **6a–f**, and **7a–f** were evaluated against MCF-7 and MDA-MB-231 breast cancer cells through the MTT assay. The percentage of growth inhibition in cancer cells was assessed at various concentrations (1, 5, 10, 20, 40, 50, and 100 µM). Plumbagin and Tamoxifen were employed as a positive control, and the outcomes are depicted in Figure S1 (ESI). The IC_{50} values of the tested compounds on breast cancer cells, along with their cytotoxicity on Vero kidney epithelial cells (ATCC® CCL-81™), are presented in Table 1.

As shown in Table 1, the target compounds had insignificant IC_{50} values against MDA-MB-231 cells. On estrogen-responsive MCF-7 cells, compounds **5a, 5b, 5c, 5e, 5f, 6a, 6c, 6d, 6e, 6f, 7a–f** failed to exhibit any growth inhibitory effects. Compounds **5d** and **6b** among all the synthesised compounds showed marginally better inhibition, with respective IC_{50} values of 92.08 µM and 71.65 µM, however they were still less potent than the standard tamoxifen. SAR established that replacing the free carbonyl group of 5-methoxy derivative **5d** with thiosemicarbazone (**6d**) or semicarbazone (**7d**) resulted in a complete loss of activity. In contrast, the inclusion of thiosemicarbazone converted inactive 5-fluoro precursor **4b** to moderately active **6b**, with an IC_{50} value of 71.65 µM against MCF-7 cells. Besides improving the activity, the inclusion of thiosemicarbazone also lowered the toxicity towards normal kidney cells, as revealed by their cytotoxicity analysis. The selectivity index also showed marginal improvement with the inclusion of thiosemicarbazone as evident by comparing the SI of **5d** with **6b**.

A critical role of iron (Fe) is observed in its catalytic function within Ribonucleotide Reductase (RNR), which harbours a di-Fe centre at its active (R2) site. This site is instrumental in facilitating the crucial step of DNA synthesis by transforming ribonucleotide precursors into deoxyribonucleotides [28]. Neoplastic cells, characterized by increased rates of proliferation and DNA synthesis, exhibit a heightened demand for active RNR and consequently for Fe [29, 30]. Consequently, it was deemed valuable to conduct preliminary spectral and electrochemical studies of the moderately active thiosemicarbazone **6b** in the presence of biologically relevant metal ions like Fe^{3+} and Fe^{2+}. Furthermore, these investigations were expanded to encompass Cu^{2+}, Zn^{2+}, Ni^{2+}, and Co^{2+} ions for a thorough analysis.

Table 1 IC_{50}^{a} value of the test compounds in MCF-7 and MDA-MB-231 breast cancer cells and cytotoxicity analysis on Vero kidney epithelial cells

Code	R^1	R^2	IC_{50}^{a}(µM)		IC_{50}^{b}(µM)	SI[c]
			MCF-7	MDA-MB-231	Cytotoxicity	
5a	H	H	> 100	> 100	> 100	–
5b	F	H	> 100	> 100	> 100	–
5c	Cl	H	> 100	> 100	59.9	–
5d	OMe	H	**92.08**	> 100	> 100	> 1.08
5e	Br	H	> 100	> 100	48.63	–
5f	Br	Br	> 100	> 100	–	–
6a	H	H	> 100	> 100	> 100	–
6b	F	H	**71.65**	> 100	> 100	> 1.39
6c	Cl	H	> 100	> 100	> 100	–
6d	OMe	H	> 100	> 100	> 100	–
6e	Br	H	> 100	> 100	> 100	–
6f	Br	Br	> 100	–	–	–
7a	H	H	> 100	> 100	> 100	–
7b	F	H	> 100	> 100	> 100	–
7c	Cl	H	> 100	> 100	> 100	–
7d	OMe	H	> 100	> 100	> 100	–
7e	Br	H	> 100	> 100	> 100	–
7f	Br	Br	> 100	–	–	–
Tamoxifen			17.71	69.67		
Plumbagin			3.5	4.4		

IC_{50}^{a} 50% inhibitory concentration (µM) on breast cancer (MCF-7/MDA-MB-231) cells

IC_{50}^{b} 50% inhibitory concentration (µM) on Vero Kidney cells

SI[c] Selectivity index (IC_{50}^{b} (Vero kidney cells)/IC_{50}^{a} (MCF-7 cells))

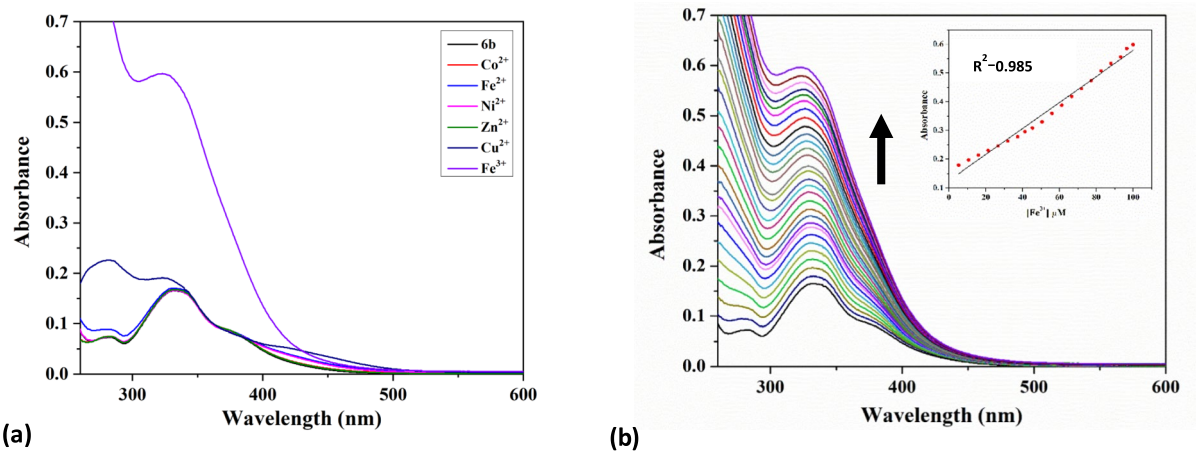

Fig. 2 **a** UV–Visible spectra of **6b** (5 µM in DMSO) in the presence of different metal ions (20 equiv. each in DMSO) **b** Absorption behaviour of **6b** (5 µM in DMSO) upon successive addition of Fe^{3+}; Inset: Calibration plot of absorbance vs [Fe^{3+}]

2.3 Spectroscopic and Electrochemical Investigation

2.3.1 UV–Vis Spectral Studies

UV–Vis spectrum of **6b** (5 µM in DMSO) showed two distinct absorption maxima at 280 and 332 nm and a shoulder at 372 nm. The band at 280 nm can be assigned to π–π^* transitions of aromatic rings while the band at 332 nm corresponds to n–π^* transitions of azomethine and thioamide region of thiosemicarbazones (Fig. 2a) [31]. The chromogenic behaviour of **6b** was screened in the presence of 20 equivalents of different biologically active metal ions (Co^{2+}, Fe^{2+}, Ni^{2+}, Zn^{2+}, Cu^{2+} and Fe^{3+}). No significant spectral changes were observed for the metal ions tested except Fe^{3+}, thereby revealing its sensitivity for Fe^{3+} (Fig. 2a). Further, the absorption titration was carried out with progressive additions of Fe^{3+} (0–100 µM) into the solution of **6b** (5 µM in DMSO) and the absorption bands were found to show continuous increase in intensity with blue shift of band at 332 nm to 323 nm which may be attributed to the interaction of azomethine nitrogen with Fe^{3+} (Fig. 2b). The plot drawn between absorbance at 332 nm and concentration of Fe^{3+} represent linear change in concentration range from 5.33 to 100 µM with detection limit of 0.38 µM. The strength of binding between **6b** and Fe^{3+} was further examined using Benesi and Hildebrand's (B–H) graphical method which involved plot of the change in absorption intensity ($1/A - A_O$) vs. 1/[Fe^{3+}]. The BH plot (Figure S2 in supporting information) showed good linearity with regression coefficient of 0.996 and confirmed 1:1 stoichiometry between **6b** and Fe^{3+}. The association constant (K_a) was calculated to be 4.1×10^3 M^{-1} which is adequately high to confirm exceptional binding capacity and sensitivity of **6b** towards Fe^{3+}.

2.3.2 Electrochemical Studies

Voltammetry techniques such as Cyclic voltammetry (CV) and Differential Pulse Voltammetry (DPV) provides comprehensive and valuable information about the redox nature of a compound and can be used to explore their binding interactions with biologically active metal ions which may also be helpful for investigating then prospective drug candidature of that compound. In the present work, the electrochemical behaviour of **6b** (5×10^{-4} M) towards Fe^{3+} was investigated using CV and DPV at glassy carbon electrode (GCE) in 0.01 M TBAP/DMSO at a scan rate of 50 mV/sec in the potential range from − 2.6 to − 1.0 V. The cyclic voltammogram of **6b** (Fig. 3a) showed two peaks at − 1.81 and − 2.35 V which can be attributed to the reduction of imine and thioamide groups, respectively. Upon addition of 5 equivalents of Fe^{3+}, the peaks showed cathodic shift to − 1.84 and − 2.38 V which might be due to the complexation between **6b** and Fe^{3+}. To further gain insight into the binding mechanism of **6b** with Fe^{3+}, **6b** was subjected to DPV measurements as this technique provides better peak resolution as compared to CV. DPV of **6b** (5×10^{-4} M) showed two intense peaks at − 1.77 and − 2.31 V which in the presence of Fe^{3+} shifted to 1.81 V and − 2.37 V, respectively (Fig. 3b). Further, to confirm the electrochemical recognition sensitivity of **6b**, voltametric titration was performed with sequential addition of Fe^{3+} (up to 5 equiv.) into the solution of **6b** (5×10^{-4} M). The increase in concentration of Fe^{3+} significantly affected peak currents and peak potentials of **6b** as shown in Fig. 4. With addition of each aliquot of Fe^3, the peaks showed increase in current intensity along with cathodic shift in peak potential to − 1.81 V and − 2.37 V and appearance of shoulders at − 1.60 and − 1.97 V. These changes may be attributed to the interaction

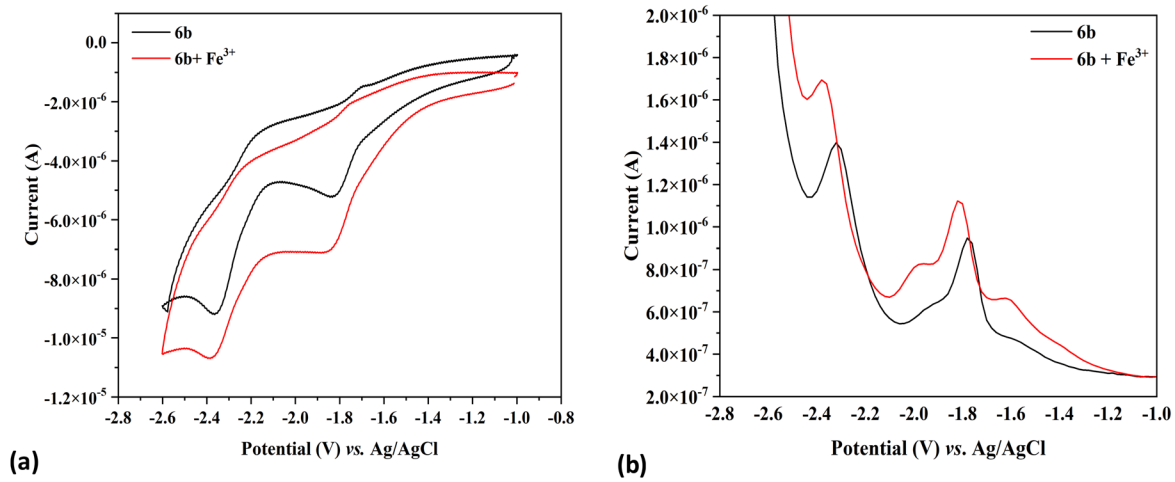

Fig. 3 **a** Cyclic Voltammograms of **6b** (5×10^{-4} M) and **6b** (5×10^{-4} M) + Fe^{3+} (5 equiv.) in DMSO. Supporting electrolyte: 0.01 M TBAP; Scan rate: 50 mV/sec; **b** Differential Pulse Voltammograms (DPV) of **6b** (5×10^{-4} M) and **6b** (5×10^{-4} M) + Fe^{3+}(5 equiv.) in DMSO. Supporting electrolyte: 0.01 M TBAP; Pulse amplitude: 0.05 V; Pulse width: 0.05 s; Pulse period: 0.5 s

of Fe^{3+} with **6b** and lead to the confirmation of **6b** + Fe^{3+} complex formation.

Considering experimental evidences, we were able to establish that introducing thiosemicarbazone to the inactive and cytotoxic **5b** culminated in **6b**, a non-cytotoxic RNR inhibitor with Fe(III) chelation ability (Fig. 5).

2.4 Molecular Docking

Ribonucleotide Reductase (RNR) plays a vital role in converting ribonucleoside diphosphates (RNDPs) to deoxyribonucleoside diphosphates (DNDPs), a critical step in maintaining nucleotide balance for DNA synthesis. Its elevated expression during the S-phase of the cell cycle makes it a promising target for anti-proliferative drugs, including cancer therapeutics [32]. The selected RNR target (PDB ID: 2EUD) corresponds to yeast ribonucleotide reductase, a key enzyme in DNA synthesis and repair. Due to its structural and functional similarity to human RNR, it serves as a useful model for studying inhibitor binding and enzyme dynamics [33].

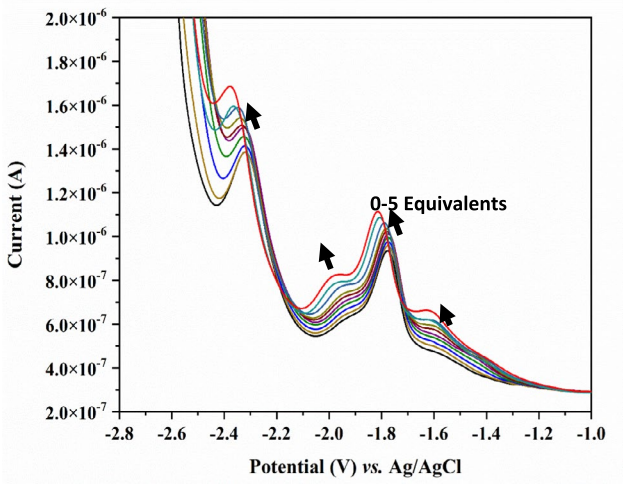

Fig. 4 Differential Pulse Voltammograms (DPV) of 5×10^{-4} M **6b** in DMSO in presence of Fe^{3+}. Supporting electrolyte: 0.01 M TBAP; Pulse amplitude: 0.05 V; Pulse width: 0.05 s; Pulse period: 0.5 s

We conducted in-silico studies to investigate the interactions of the unique binding core of ribonucleotide reductase (RNR) (PDB ID: 2EUD) with compounds—**5b (inactive)** and **6b (active)**. The results obtained were compared to triapine, a thiosemicarbazide based RNR inhibitor chosen as standard The docking results demonstrated that both **5b** and **6b** exhibited favourable binding modes, successfully occupying the protein's active site as depicted in Fig. 6. Additionally, we summarized the docking calculations for **5b**, **6b**, and Triapine in Table 2. Specifically, the docking score for **5b** was determined to be − 9.227, whereas for **6b** and the reference drug, it was found to be − 5.480 and − 4.798, respectively.

For compound **5b**, the carbonyl oxygen located at the C-3 position of isatin was involved in two out of the four hydrogen bonding interactions observed, forming bonds with SER610 and THR611. The remaining two hydrogen bonds were noted between SER202 and the carbonyl oxygen at the C-4 position of isatin. Additionally, two polar interactions were observed: a dipole-induced dipole interaction between the C-6 of benzaldehyde and the carbonyl group of ASP291, and an induced dipole-induced dipole interaction between the aldehydic carbon and the PHE206 amino acid residue. In the case of compound **6b**, there was a π-cation interaction observed between ARG293 and the triazole ring.

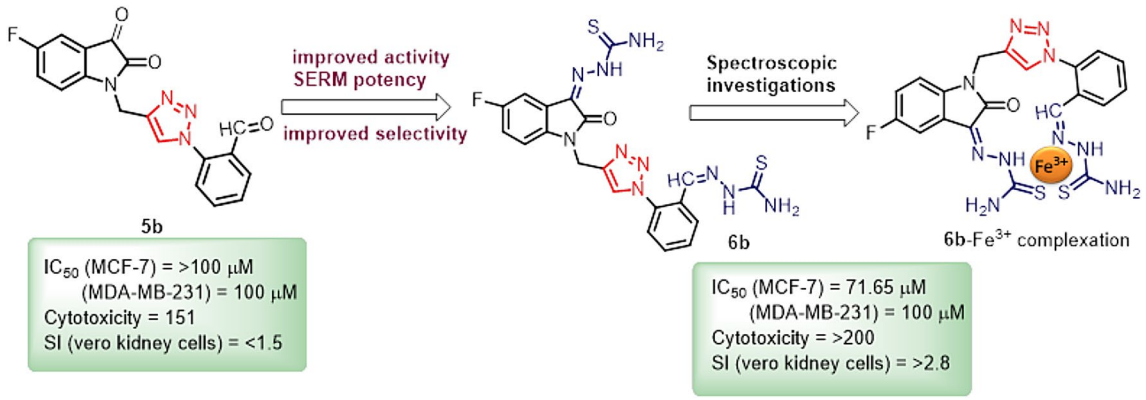

Fig. 5 Inclusion of thiosemicarbazone to inactive **5b** produced Fe (III) chelator and a potential RNR inhibitor, **6b**

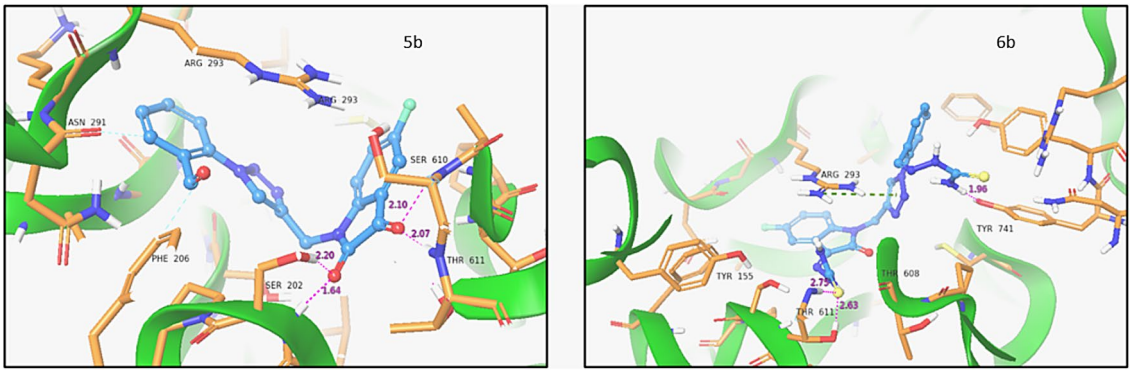

Fig. 6 3D representation of RNR protein–Ligand interaction for compound **5b** and **6b**

Additionally, three hydrogen bonds were identified: one between NH_2 and TYR741 and another two between thione and THR611 (Fig. 6).

Furthermore, the study revealed that compound **5b** exhibited the highest number of interactions. However, replacing the carbonyl group at the C-3 position of isatin with a thiosemicarbazide moiety led to reduced interactions. This decrease in binding affinity is reflected in the lower docking score, suggesting that the carbonyl group plays a crucial role in stabilizing interactions with the target protein. The substitution likely alters the electronic environment and spatial orientation, thereby weakening key interactions essential for strong ligand–protein binding.

However, the molecular docking investigations have revealed that both **5b** and **6b** exhibited higher docking scores in comparison to Triapine suggesting that these compounds displayed more favorable interactions with the protein, implying their potential as ribonucleotide reductase (RNR) inhibitors.

Table 2 Docking calculations of compounds **5b, 6b,** and Triapine

Ligand	Docking score	XPGScore	Glide emodel
5b	− 9.227	− 9.227	− 61.422
6b	− 5.480	− 5.480	− 87.203
Triapine	− 4.798	− 4.798	− 46.401

2.5 ADMET Studies

ADMET (Absorption, Distribution, Metabolism, Excretion, and Toxicity) studies were conducted to comprehensively assess the safety profile, efficacy, and physicochemical properties of the most potent compound of the series, **6b**. The ADMET descriptor module of small molecules was utilized for ADMET prediction, accessible at http://www.swissadme.ch/ and http://biosig.unimelb.edu.au/pkcsm/prediction. The acquired values are presented in Table S1 of the supplementary data. These studies revealed that compound **6b** exhibited the potential to act as a P-glycoprotein inhibitor. This property can enhance the bioavailability of drugs and improve their uptake in targeted organs. None of the CYP450 isoforms were inhibited by **6b** indicating rapid metabolism and clearance from the biological system. Importantly, this reduces the likelihood of adverse effects resulting from drug–drug

interactions. However, one notable limitation was observed in the form of poor lipophilicity, with a Log *P* value of 1.49, and a low diffusion parameter, represented as Log BB = − 1.351. These characteristics suggest that the synthesized compounds may face challenges in crossing the blood–brain barrier (BBB) and their inability to efficiently traverse the lipid bilayer that could explain the observed limited activity. This poor lipophilicity may hinder their ability to reach and interact with the intended target sites.

3 Conclusion

This manuscript details the design and synthesis of indolin-2-one-bis(thiosemicarbazones/semicarbazones) linked by 1*H*-1,2,3-triazole. The anti-proliferative activity of these compounds was assessed against MCF-7 and MDA-MB-231 breast cancer cells. Notably, compounds **5d** and **6b** exhibited slightly stronger inhibition, demonstrating IC_{50} values of 92.08 μM and 71.65 μM against MCF-7 cell lines, respectively. Spectroscopic and electrochemical analyses indicated that compound **6b** has the potential to bind to Fe(III), a crucial regulator in the activity of ribonucleotide reductase. Molecular docking studies further highlighted that **6b** surpasses the reference drug triapine in binding interactions with the RNR. Nevertheless, further optimization is required to enhance the anti-proliferative effectiveness of **6b** to reach the level of efficacy seen with Tamoxifen.

4 Experimental Section

4.1 General Synthetic Protocols

The standard protocols and techniques were used to carry out all the reactions. The column chromatography was carried out using silica gel (60–120 mesh) with ethyl acetate: hexane as eluent. Melting points were recorded by using open capillaries and are uncorrected. The spectra of ^{1}H NMR and ^{13}C NMR spectra were recorded on JEOL400 and 100 MHz spectrometers and were obtained as $CDCl_3$ solutions relative to tetramethylsilane (TMS) as an internal standard. Chemical shifts were reported in parts per million(ppm) and coupling constants J were indicated in hertz. Splitting patterns are indicated as s: singlet, d: doublet, t: triplet, m: multiplet, dd: double of doublet, ddd: doublet of a doublet of a doublet, and br: broad peak. Mass spectral data was assembled on Bruker-micrOTOF QII equipment using ESI as the source. IR spectra were recorded on the Shimadzu IRAffinity-1 Fourier Transform Infrared (FTIR) spectrophotometer.

4.2 General Procedure for the Synthesis of 5a–f

To synthesize precursors **5a–f**, a catalytic amount of $CuSO_4 \cdot 5H_2O$ (0.055 mmol) and sodium ascorbate (0.143 mmol) were added to a well-stirred solution of *O*-azidobenzaldehyde **4** (1 mmol) and C-5 substituted *N*-propargylated isatin **2** (1 mmol) in EtOH: H_2O (8:2) mixture. The reaction was carried out at room temperature for 7–8 h and monitored by TLC. On completion, the reaction mixture was extracted with chloroform (2 × 30 mL) and water (2 × 25 mL). The organic layer was dried over anhydrous Na_2SO_4 and concentrated under reduced pressure to yield the desired conjugates **5a–f.** The resulting compounds were purified via column chromatography technique using silica gel (60–120 mesh) as the stationary phase and ethylacetate:hexane (7:3) as the eluent mixture.

4.2.1 2-[4-(2,3-Dioxo-2,3-dihydro-indol-1-ylmethyl)-[1,2,3] triazol-1-yl]-benzaldehyde (5a)

Yield 89%, light orange solid, MP = 193–196 °C, IR (KBr, ν_{max}/cm^{-1}): 3136 (C–H triazole); 1735 (–CHO); 1739 (C=O); 1692 (–N–C=O), ^{1}H NMR (400 MHz, $CDCl_3$) δ 5.12 (s, 2H, $–CH_2$); 7.13 (td, J = 0.9, 7.5 Hz, 1H, Ar–H); 7.36 (d, J = 8.0 Hz, 1H, Ar–H); 7.46 (dd, J = 1.3, 7.9 Hz, 1H, Ar–H); 7.58–7.67 (m, 3H, Ar–H); 7.74 (td, J = 1.6, 7.5 Hz, 1H, Ar–H); 8.06–8.08 (m, 2H, Ar–H + triazole-H); 9.85 (d, J = 0.92 Hz, 1H, –CHO). ^{13}C NMR (100 MHz, $CDCl_3$) δ 35.3, 111.4, 117.6, 124.3, 125.1, 125.4, 125.6, 129.9, 130.3, 130.4, 134.8, 137.8, 138.8, 142.5, 150.1, 158.1, 183.0, 188.4. HRMS (ESI) calcd for $C_{18}H_{12}N_4O_3$ $[M+H]^+$ 333.0943, found 333.0721.

4.2.2 2-[4-(5-Fluoro-2,3-dioxo-2,3-dihydro-indol-1-ylmethyl)-[1,2,3]triazol-1-yl]-benzaldehyde (5b)

Yield 87%, light brown solid, MP = 197–199 °C, IR (KBr, ν_{max}/cm^{-1}): 3142 (C–H triazole); 1751 (–CHO); 1732 (C=O); 1697 (–N–C=O), ^{1}H NMR (400 MHz, $CDCl_3$) δ5.15 (s, 2H, $–CH_2$); 7.33–7.44 (m, 3H, Ar–H); 7.51 (d, J = 6.3 Hz, 1H, Ar–H); 7.70 (t, J = 6.0 Hz, 1H, Ar–H); 7.78 (t, J = 6.0 Hz, 1H, Ar–H); 8.09 (s, 1H, triazole-H); 8.11 (d, J = 6.1 Hz, 1H, Ar–H); 9.90 (s, 1H, –CHO). ^{13}C NMR (100 MHz, $CDCl_3$) δ 35.3, 112.3, 112.5, 112.7 (J = 5.7 Hz), 118.2 (J = 5.6 Hz), 124.9, 125.1 (J = 3.6 Hz), 125.4, 130.1, 130.3 (J = 5.5 Hz), 134.6, 137.6, 142.2, 146.1, 157.7 (J = 80.8 Hz), 160.5, 182.3, 188.1. HRMS (ESI) calcd for $C_{18}H_{11}FN_4O_3$ $[M+H]^+$ 351.0849, found 351.0687.

4.2.3 2-[4-(5-Chloro-2,3-dioxo-2,3-dihydro-indol-1-ylmethyl)-[1,2,3]triazol-1-yl]-benzaldehyde (5c)

Yield 88%, yellow solid, MP = 190–193 °C, IR (KBr, ν_{max}/cm^{-1}): 3138 (C–H triazole); 1751 (–CHO); 1697 (–N–C=O); 1653(C=O), ^{1}H NMR (400 MHz, $CDCl_3$) δ5.12 (s, 2H, $–CH_2$); 7.35–7.47 (m, 3H, Ar–H); 7.53 (d, J = 6.5 Hz, 1H, Ar–H); 7.72 (t, J = 6.4 Hz, 1H, Ar–H); 7.79 (t, J = 6.1 Hz, 1H, Ar–H); 8.11 (s, 1H, triazole-H); 8.13 (d, J = 6.1 Hz, 1H, Ar–H); 9.91 (s, 1H, –CHO). ^{13}C NMR (100 MHz, $CDCl_3$) δ 35.5, 111.1, 117.7, 124.4, 125.2, 125.5, 125.7, 129.8, 1302, 130.5, 134.9, 137.7, 138.7, 142.6, 150.2, 158.2, 183.1, 188.5. HRMS (ESI) calcd for $C_{18}H_{11}ClN_4O_3$ $[M+H]^+$ 367.0520, found 367.0671.

4.2.4 2-[4-(5-Bromo-2,3-dioxo-2,3-dihydro-indol-1-ylmethyl)-[1,2,3]triazol-1-yl]-benzaldehyde (5d)

Yield 86%, light brown solid, MP = 197–201 °C, IR (KBr, ν_{max}/cm^{-1}): 3138 (C–H triazole); 1747 (–CHO); 1737 (C=O); 1697 (–N–C=O), ^{1}H NMR (400 MHz, $CDCl_3$) δ5.10 (s, 2H, $–CH_2$); 7.17 (d, J = 8.4 Hz, 1H, Ar–H); 7.36 (d, J = 7.8 Hz, 1H, Ar–H); 7.47 (d, J = 7.8 Hz, 1H, Ar–H); 7.62–7.67 (m, 2H, Ar–H); 7.78 (d, J = 7.8 Hz, 1H, Ar–H); 8.06–8.09 (m, 2H, Ar–H + triazole-H); 9.85 (d, J = 0.94 Hz, 1H, –CHO). ^{13}C NMR (100 MHz, $CDCl_3$) δ 35.1, 111.5, 117.8, 124.2, 125.2, 125.5, 125.7, 129.9, 130.2, 130.5, 134.7, 137.9, 138.8, 142.6, 150.1, 158.2, 183.1, 188.4. HRMS (ESI) calcd for $C_{18}H_{11}BrN_4O_3$ $[M(^{79}Br)+H]^+$ 411.0015 and $[M(^{81}Br)+H]^+$ 413.0015, found 411.0032 and 413.0029.

4.2.5 2-[4-(5-Methoxy-2,3-dioxo-2,3-dihydro-indol-1-ylmethyl)-[1,2,3]triazol-1-yl]-benzaldehyde (5e)

Yield 84%, Maroon solid, MP = 195–198 °C, IR (KBr, ν_{max}/cm^{-1}): 3140 (C–H triazole); 1745 (–CHO); 1739 (C=O); 1685 (–N–C=O), ^{1}H NMR (400 MHz, $CDCl_3$) δ 3.72 (s, 3H, $–OCH_3$); 5.06 (s, 2H, $–CH_2$); 7.12 (d, J = 7.7 Hz, 1H, Ar–H); 7.39 (d, J = 7.8 Hz, 1H, Ar–H); 7.47 (dd, J = 1.2, 7.8 Hz, 1H, Ar–H); 7.55–7.64 (m, 2H, Ar–H); 7.74 (d, J = 7.7 Hz, 1H, Ar–H); 8.04–8.07 (m, 2H, Ar–H + triazole-H); 9.84 (s, 1H, –CHO). ^{13}C NMR (100 MHz, $CDCl_3$) δ 35.3, 56.1, 111.3, 117.6, 124.2, 125.3, 125.5, 125.7, 129.9, 130.1, 130.5, 134.9, 137.7, 138.8, 142.4, 150.2, 158.2, 183.1, 188.4. HRMS (ESI) calcd for $C_{19}H_{14}N_4O_4$ $[M+H]^+$ 363.1049, found 363.1011.

4.2.6 2-(4-((5,7-dibromo-2,3-dioxoindolin-1-yl)methyl)-1H-1,2,3-triazol-1-yl)benzaldehyde (5f)

Yield 80%, brown solid, MP = 138–140 °C, IR (KBr, ν_{max}/cm^{-1}): 3138 (C–H triazole); 1732 (–CHO); 1714 (C=O); 1689 (–N–C=O), ^{1}H NMR (400 MHz, $CDCl_3$) δ 5.12 (s, 2H, $–CH_2$); 7.15 (d, J = 8.3 Hz, 1H, Ar–H); 7.32 (d, J = 7.8 Hz, 1H, Ar–H); 7.43 (d, J = 7.8 Hz, 1H, Ar–H); 7.59 (s, 1H, Ar–H); 7.78 (d, J = 7.8 Hz, 1H, Ar–H); 8.07–8.10 (m, 2H, Ar–H + triazole-H); 9.87 (s, 1H, –CHO). ^{13}C NMR (100 MHz, $CDCl_3$) δ 35.3, 111.7, 118.2, 125.0, 125.2, 125.7, 125.9, 128.9, 130.1, 130.4, 134.8, 137.4, 138.7, 141.9, 150.4, 157.9, 183.2, 188.3. HRMS (ESI) calcd for $C_{18}H_{10}Br_2N_4O_3$ $[M(^{79}Br)+H]^+$ 488.9120 and $[M(^{81}Br)+H]^+$ 490.9099, found 488.9157 and 490.9043.

4.3 General Procedure for the Synthesis of Schiff Bases 6a–f/7a–f

Compound **5** (1 mmol) and thiosemicarbazide/semicarbazide (2 mmol) were dissolved in a minimum quantity of warm ethanol and a catalytic amount of glacial acetic acid (0.1 mL) was added to the mixture. The reaction mixture was refluxed for 6 h and allowed to cool down at room temperature. The solid precipitated out which was filtered, washed, dried, and recrystallized from ethanol to obtain desired compounds **6a–f/7a–f** in excellent yields.

4.3.1 2-((E)-2-(4-(((Z)-3-(2-carbamothioylhydrazono)-2-oxoindolin-1-yl)methyl)-1H-1,2,3-triazol-1-yl)benzylidene)hydrazine-1-carbothioamide (6a)

Yield 85%, pale yellow solid, MP = 244–247 °C, IR (KBr, ν_{max}/cm^{-1}): 3419 (–NH); 3153(C–H triazole); 1685 (–N–C=O); 1608 (–C=N); 1180–1278 (C=S), ^{1}H NMR (400 MHz, DMSO-d_6) δ 5.10 (s, 2H, $–CH_2$); 7.21 (d, J = 8.6 Hz, 1H, Ar–H); 7.42–7.46 (m, 2H, Ar–H); 7.48–7.54 (m, 3H, Ar–H); 7.73 (s, 1H, –NH (exchangeable with D_2O)); 7.77 (d, J = 2.9 Hz, 1H, Ar–H); 8.00 (s, 1H, triazole-H); 8.24 (s, 1H, –CH=N); 8.35–8.38 (m, 1H, Ar–H); 8.54 (s, 1H, –NH (exchangeable with D_2O)); 8.68 (s, 1H, –NH (exchangeable with D_2O)); 9.15 (s, 1H, –NH (exchangeable with D_2O)); 11.46 (s, 1H, –NH(exchangeable with D_2O)); 12.12 (s, 1H, –NH(exchangeable with D_2O)). ^{13}C NMR (100 MHz, DMSO-d_6) δ 35.1, 107.9, 112.4, 117.8, 121.0, 126.3, 126.7, 127.5, 129.9, 130.1, 130.4, 130.7, 135.8, 137.6, 139.4, 142.4, 158.3, 160.7, 178.4, 179.1. HRMS (ESI) calcd for $C_{20}H_{18}N_{10}OS_2$ $[M+H]^+$ 479.1140, found 479.1019.

4.3.2 2-((Z)-5-fluoro-1-((1-(2-((E)-(2-carbamothioylhydrazono)methyl)phenyl)-1H-1,2,3-triazol-4-yl)methyl)-2-oxoindolin-3-ylidene)hydrazine-1-carbothioamide (6b)

Yield 86%, pale yellow solid, MP = 245–248 °C, IR (KBr, ν_{max}/cm^{-1}): 3469 (–NH); 3132 (C–H triazole); 1693 (–N–C=O); 1606 (C=N); 1141–1228 (C=S), ^{1}H NMR (500 MHz, DMSO-d_6) δ5.16 (s, 2H, –CH_2); 7.26–7.32 (m, 2H, Ar–H); 7.48 (d, J = 7.0 Hz, 1H, Ar–H); 7.56–7.60 (m, 3H, Ar–H); 7.76 (s, 1H, –NH (exchangeable with D_2O)); 8.01 (s, 1H, triazole-H); 8.29 (s, 1H, –CH=N); 8.41 (d, J = 7.8 Hz, 1H, Ar–H); 8.61 (s, 1H, –NH (exchangeable with D_2O)); 8.85 (s, 1H, –NH (exchangeable with D_2O); 9.20 (s, 1H, –NH (exchangeable with D_2O); 11.45 (s, 1H, –NH (exchangeable with D_2O,); 12.29 (s, 1H, –NH (exchangeable with D_2O)). ^{13}C NMR (125 MHz, DMSO-d_6) δ35.1, 108.3 (J = 25.7 Hz), 112.2 (J = 8.0 Hz), 117.7, 117.8, 126.4, 126.7, 127.4, 129.9, 130.3, 130.6 (J = 3.1 Hz), 130.8, 135.9, 137.6, 139.1, 142.3, 158.2, 160.5 (J = 96.2 Hz), 178.6, 179.2. HRMS (ESI) calcd for $C_{20}H_{17}FN_{10}OS_2$ $[M+H]^+$ 497.1046, found 497.1298.

4.3.3 2-((Z)-5-chloro-1-((1-(2-((E)-(2-carbamothioylhydrazono)methyl)phenyl)-1H-1,2,3-triazol-4-yl)methyl)-2-oxoindolin-3-ylidene)hydrazine-1-carbothioamide (6c)

Yield 85%, pale yellow solid, MP = 215–218 °C, IR (KBr, ν_{max}/cm^{-1}): 3161–3147 (–NH); 3134 (C–H triazole); 1697 (–N–C=O); 1653 (C=N); 1120 (C=S), ^{1}H NMR (400 MHz, DMSO-d_6) δ 5.11 (s, 2H, –CH_2); 7.23 (d, J = 8.7 Hz, 1H, Ar–H); 7.42–7.45 (m, 2H, Ar–H); 7.50–7.56 (m, 2H, Ar–H); 7.70 (s, 1H, –NH (exchangeable with D_2O)); 7.78 (d, J = 2.7 Hz, 1H, Ar–H); 8.00 (s, 1H, triazole-H); 8.27 (s, 1H, –CH=N); 8.35–8.38 (m, 1H, Ar–H); 8.56 (s, 1H, –NH (exchangeable with D_2O)); 8.86 (s, 1H, –NH (exchangeable with D_2O)); 9.17 (s, 1H, –NH (exchangeable with D_2O)); 11.42 (s, 1H, –NH(exchangeable with D_2O)); 12.17 (s, 1H, –NH(exchangeable with D_2O)) ^{13}C NMR (100 MHz, DMSO-d_6) δ 35.1, 112.6, 121.0, 121.9, 126.5, 126.8, 127.4, 127.9, 129.9, 130.1, 130.4, 130.9, 136.0, 137.6, 141.5, 142.4, 160.7, 178.5, 179.2. HRMS (ESI) calcd for $C_{20}H_{17}ClN_{10}OS_2$ $[M+H]^+$ 513.0717, found 513.0732.

4.3.4 2-((Z)-5-bromo-1-((1-(2-((E)-(2-carbamothioylhydrazono)methyl)phenyl)-1H-1,2,3-triazol-4-yl)methyl)-2-oxoindolin-3-ylidene)hydrazine-1-carbothioamide (6d)

Yield 85%, pale yellow solid, MP = 258–261 °C, IR (KBr, ν_{max}/cm^{-1}): 3158–3449 (–NH); 3132 (C–H triazole); 1698 (–N–C=O); 1657 (–C=N); 1120 (C=S), ^{1}H NMR (400 MHz, DMSO-d_6) δ 5.12 (s, 2H, –CH_2); 7.21 (d, J = 8.6 Hz, 1H, Ar–H); 7.46–7.50 (m, 2H, Ar–H); 7.53–7.57 (m, 2H, Ar–H); 7.74 (s, 1H, –NH (exchangeable with D_2O)); 7.79 (d, J = 2.6 Hz, 1H, Ar–H); 8.02 (s, 1H, triazole-H); 8.31 (s, 1H, –CH=N); 8.37–8.39 (m, 1H, Ar–H); 8.58 (s, 1H, –NH (exchangeable with D_2O)); 8.71 (s, 1H, –NH (exchangeable with D_2O)); 9.21 (s, 1H, –NH (exchangeable with D_2O)); 11.43 (s, 1H, –NH(exchangeable with D_2O)); 12.19 (s, 1H, –NH(exchangeable with D_2O)). ^{13}C NMR (100 MHz, DMSO-d_6) δ 35.2, 117.2, 121.3, 121.9, 126.7, 126.9, 127.4, 127.9, 129.8, 130.1, 130.4, 130.8, 136.1, 137.6, 139.9, 142.4, 158.1, 160.8, 178.5, 179.1. HRMS (ESI) calcd for $C_{20}H_{17}BrN_{10}OS_2$ $[M(^{79}Br)+H]^+$ 557.0212 and $[M(^{81}Br)+H]^+$ 559.0212, found 557.0229 and 559.0222.

4.3.5 2-((E)-2-(4-(((E)-3-(2-carbamoylhydrazono)-5-methoxy-2-oxoindolin-1-yl)methyl)-1H-1,2,3-triazol-1-yl)benzylidene)hydrazine-1-carbothiomide (6e)

Yield 84%, light maroon solid, MP = 241–244 °C, IR (KBr, ν_{max}/cm^{-1}): 3159–3441 (–NH); 3126 (C–H triazole); 1689 (–N–C=O); 1531–1604 (–C=N); 1128–1220 (C=S), ^{1}H NMR (400 MHz, DMSO-d_6) δ 3.72 (s, 3H, –OCH_3); 5.07 (s, 2H, –CH_2); 6.95 (d, J = 10.0 Hz, 1H, Ar–H); 7.11 (d, J = 8.6 Hz, 1H, Ar–H); 7.36 (s, 1H, Ar–H); 7.42–7.44 (m, 1H, Ar–H); 7.52–7.54 (m, 2H, Ar–H); 7.70 (s, 1H, –NH (exchangeable with D_2O)); 8.00 (s, 1H, triazole-H); 8.27 (s, 1H, –CH=N); 8.37 (d, J = 8.2 Hz, 1H, Ar–H); 8.56 (s, 1H, –NH (exchangeable with D_2O)); 8.78 (s, 1H, –NH (exchangeable with D_2O));); 9.11 (s, 1H, –NH (exchangeable with D_2O));); 11.43 (s, 1H, –NH (exchangeable with D_2O)); 12.30 (s, 1H, –NH (exchangeable with D_2O)) ^{13}C NMR (100 MHz, DMSO-d_6) δ 35.0, 56.1, 106.8, 111.8, 117.3, 120.9, 126.5, 126.8, 127.4, 129.9, 130.4, 130.9, 131.6, 136.0, 136.6, 137.6, 142.6, 156.3, 160.9, 178.6, 179.1. HRMS (ESI) calcd for $C_{21}H_{20}N_{10}O_2S_2$ $[M+H]^+$ 509.1246, found 509.1261.

4.3.6 2-(E)-2-(5,7-dibromo-1-((1-(2-((E)-(2-carbamothioylhydrazono)methyl)phenyl)-1H-1,2,3-triazol-4-yl)methyl)-2-oxoindolin-3-ylidene)hydrazinecarbothioamide (6f)

Yield 81%, yellow solid, MP = 238–240 °C, IR (KBr, ν_{max}/cm^{-1}): 3159–3419 (–NH); 3134 (C–H triazole); 1693 (–N–C=O); 1541–1600 (–C=N); 1134–1271 (C=S), ^{1}H NMR (400 MHz, DMSO-d_6) δ 5.12 (s, 2H, –CH_2); 6.98 (d, J = 8.4 Hz, 1H, Ar–H); 7.49–7.51 (m, 2H, Ar–H); 7.56–7.59 (m, 1H, Ar–H); 7.72 (s, 1H, –NH (exchangeable with D_2O)); 7.81 (d, J = 2.2 Hz, 1H, Ar–H); 8.01 (s, 1H, triazole-H); 8.32 (s, 1H, –CH=N); 8.39 (s, 1H, Ar–H); 8.57 (s, 1H, –NH (exchangeable with D_2O)); 8.73 (s, 1H, –NH

(exchangeable with D_2O)); 9.22 (s, 1H, –NH (exchangeable with D_2O)); 11.41 (s, 1H, –NH(exchangeable with D_2O)); 12.27 (s, 1H, –NH(exchangeable with D_2O)). ^{13}C NMR (100 MHz, DMSO-d_6) δ 35.1, 118.1, 119.3, 121.8, 126.4, 126.9, 127.3, 127.8, 129.7, 130.3, 130.5, 131.4, 136.8, 137.3, 139.8, 142.6, 158.2, 160.7, 178.6, 179.1. HRMS (ESI) calcd for $C_{20}H_{16}Br_2N_{10}OS_2$ [M(^{79}Br) + H]$^+$ 634.9317 and [M(^{81}Br) + H]$^+$ 636.9296 found 634.9209 and 636.925.

4.3.7 2-((E)-2-(4-(((Z)-3-(2-carbamothioylhydrazono)-2-oxoindolin-1-yl)methyl)-1H-1,2,3-triazol-1-yl)benzylidene)hydrazine-1-carboxamide (7a)

Yield 84%, pale yellow solid, MP = 262–265 °C, IR (KBr, ν_{max}/cm^{-1}): 3471 (–NH_2); 3151 (C–H triazole); 1714 (C=O); 1697 (–N–C=O); 1681 (C=O); 1608 (C=N), ^1H NMR (400 MHz, DMSO-d_6) δ 5.12 (s, 2H, –CH_2); 6.45 (s, 2H, –NH_2(exchangeable with.

(d, J = 7.7 Hz, 1H, Ar–H); 7.46–7.55 (m, 5H, 3Ar–H + –NH_2 (exchangeable with D_2O)); 7.70–7.97 (m, 2H, Ar–H + triazole-H); 8.26 (d, J = 7.8 Hz, 1H, Ar–H); 8.53 (s, 1H, –CH=N); 10.25 (s, 1H, –NH (exchangeable with D_2O)); 11.46 (s, 1H, –NH (exchangeable with D_2O)). ^{13}C NMR (100 MHz, DMSO-d_6) δ 35.1, 112.6, 117.9, 121.1, 121.7, 126.5, 126.8, 127.2, 130.2, 130.5, 130.9, 134.8, 135.2, 135.9, 136.3, 142.5, 155.8, 156.4, 160.1, 161.5. HRMS (ESI) calcd for $C_{20}H_{17}BrN_{10}O_3$ [M(^{79}Br) + H]$^+$ 525.0668 and [M(^{81}Br) + H]$^+$ 527.0668, found 525.0654 and 525.0651.

4.3.8 2-((Z)-5-fluoro-1-((1-(2-((Z)-(2-carbamoylhydrazono)methyl)phenyl)-1H-1,2,3-triazol-4-yl)methyl)-2-oxoindolin-3-ylidene)hydrazine-1-carboxamide (7b)

Yield 86%, pale yellow solid, MP = 257–260 °C, IR (KBr, ν_{max}/cm^{-1}): 3288–3469 (–NH); 3132(C–H triazole); 1716 (C=O); 1685 (–N–C=O); 1608 (–C=N); ^1H NMR (400 MHz, DMSO-d_6) δ 5.11 (s, 2H, –CH_2); 6.44 (s, 2H, –NH_2(exchangeable with D_2O)); 7.18 (d, J = 8.6 Hz, 1H, Ar–H); 7.40 (d, J = 7.6 Hz, 1H, Ar–H); 7.46–7.54 (m, 4H, 2Ar–H + –NH_2 (exchangeable with D_2O)); 7.62 (d, J = 8.4 Hz, 1H, Ar–H); 7.71–7.99 (m, 2H, Ar–H + triazole-H); 8.27 (d, J = 7.9 Hz, 1H, Ar–H); 8.52 (s, 1H, –CH=N); 10.24 (s, 1H, –NH (exchangeable with D_2O)); 11.47 (s, 1H, –NH (exchangeable with D_2O)). ^{13}C NMR (100 MHz, DMSO-d_6) δ 35.1, 112.3 (J = 5.6 Hz), 117.9 (J = 7.8 Hz), 121.4, 121.9, 126.3, 127.0, 127.4, 130.1, 130.4 (J = 5.4 Hz), 130.9, 134.7, 135.2, 135.9, 136.4, 142.3, 155.7 (J = 86.7 Hz), 156.3, 156.8, 161.2. HRMS (ESI) calcd for $C_{20}H_{17}FN_{10}O_3$ [M + H]$^+$ 465.1503, found 465.1527.

4.3.9 2-((Z)-5-chloro-1-((1-(2-((Z)-(2-carbamoylhydrazono)methyl)phenyl)-1H-1,2,3-triazol-4-yl)methyl)-2-oxoindolin-3-ylidene)hydrazine-1-carboxamide (7c)

Yield 85%, pale yellow solid, MP = 252–255 °C, IR (KBr, ν_{max}/cm^{-1}): 3285–3466 (–NH); 3138 (C–H triazole); 1714 (C=O); 1697 (–N–C=O); 1683 (C=O); 1610 (–C=N), ^1H NMR (400 MHz, DMSO-d_6) δ 5.12 (s, 2H, –CH_2); 6.47 (s, 2H, –NH_2 (exchangeable with D_2O)); 7.20 (d, J = 8.6 Hz, 1H, Ar–H); 7.41 (d, J = 7.6 Hz, 1H, Ar–H); 7.44–7.54 (m, 5H, 3Ar–H + –NH_2 (exchangeable with D_2O)); 7.70–7.98 (m, 2H, Ar–H + triazole-H); 8.25 (d, J = 7.9 Hz, 1H, Ar–H); 8.51 (s, 1H, –CH=N); 10.25 (s, 1H, –NH (exchangeable with D_2O)); 11.48 (s, 1H, –NH (exchangeable with D_2O)). ^{13}C NMR (100 MHz, DMSO-d_6) δ 35.2, 112.4, 117.8, 121.0, 121.8, 126.4, 126.9, 127.3, 130.1, 130.4, 130.8, 134.9, 135.1, 135.8, 136.2, 142.4, 155.7, 156.3, 156.9, 161.1. HRMS (ESI) calcd for $C_{20}H_{17}ClN_{10}O_3$ [M + H]$^+$ 481.1174, found 481.1195.

4.3.10 2-((Z)-5-bromo-1-((1-(2-((Z)-(2-carbamoylhydrazono)methyl)phenyl)-1H-1,2,3-triazol-4-yl)methyl)-2-oxoindolin-3-ylidene)hydrazine-1-carboxamide (7d)

Yield 85%, pale yellow solid, MP = 274–277 °C, IR (KBr, ν_{max}/cm^{-1}): 3285–3468 (–NH); 3138 (C–H triazole); 1715 (C=O); 1697 (–N–C=O); 1684 (C=O); 1608 (–C=N), ^1H NMR (400 MHz, DMSO-d_6) δ 5.10 (s, 2H, –CH_2); 6.46 (s, 2H, –NH_2 (exchangeable with D_2O)); 7.17 (d, J = 8.6 Hz, 1H, Ar–H); 7.39 (d, J = 7.7 Hz, 1H, Ar–H); 7.46–7.55 (m, 5H, 3Ar–H + –NH_2 (exchangeable with D_2O)); 7.70–7.97 (m, 2H, Ar–H + triazole-H); 8.26 (d, J = 7.8 Hz, 1H, Ar–H); 8.53 (s, 1H, –CH=N); 10.25 (s, 1H, –NH (exchangeable with D_2O)); 11.46 (s, 1H, –NH (exchangeable with D_2O)). ^{13}C NMR (100 MHz, DMSO-d_6) δ 35.1, 112.6, 117.9, 121.1, 121.7, 126.5, 126.8, 127.2, 130.2, 130.5, 130.9, 134.8, 135.2, 135.9, 136.3, 142.5, 155.8, 156.4, 160.1, 161.5. HRMS (ESI) calcd for $C_{20}H_{17}BrN_{10}O_3$ [M(^{79}Br) + H]$^+$ 525.0668 and [M(^{81}Br) + H]$^+$ 527.0668, found 525.0654 and 525.0651.

4.3.11 2-((E)-2-(4-(((E)-3-(2-carbamoylhydrazono)-5-methoxy-2-oxoindolin-1-yl)methyl)-1H-1,2,3-triazol-1-yl)benzylidene)hydrazine-1-carboxamide (7e)

Yield 84%, light maroon solid, MP = 249–252 °C, IR (KBr, ν_{max}/cm^{-1}): 3381–3479 (–NH); 3138 (C–H triazole); 1714 (C=O); 1695 (–N–C=O); 1685 (C=O); 1608 (–C=N), ^1H NMR (400 MHz, DMSO-d_6) δ 3.73 (s, 3H, –OCH_3); 5.07 (s, 2H, –CH_2); 6.46 (s, 2H, –NH_2 (exchangeable with D_2O)); 6.91 (d, J = 11.4 Hz, 1H, Ar–H); 7.11 (d, J = 8.6 Hz, 1H, Ar–H); 7.19 (bs, 1H, –NH (exchangeable with D_2O)); 7.29

(s, 1H, Ar–H); 7.39 (d, $J = 7.8$ Hz, 1H, Ar–H); 7.46–7.55 (m, 4H, 2Ar–H + triazole-H + –NH (exchangeable with D_2O)); 8.26 (d, $J = 7.7$ Hz, 1H, Ar–H); 8.52 (s, 1H, –CH=N); 10.25 (s, 1H, –NH (exchangeable with D_2O)); 11.58 (s, 1H, –NH (exchangeable with D_2O)). ^{13}C NMR (100 MHz, DMSO-d_6) δ 34.9, 56.1, 106.2, 111.6, 116.5, 121.2, 126.4126.8, 127.1, 130.0, 130.4, 130.6, 130.6, 134.4, 135.3, 135.8, 142.6, 155.4, 156.3, 156.8, 161.0. HRMS (ESI) calcd for $C_{21}H_{20}FN_{10}O_4$ $[M + H]^+$ 477.1703, found 477.1727.

4.3.12 *2*-(E)-2-(5,7-dibromo-1-((1-(2-(((E)-(2-carbamoylhydrazono)methyl)phenyl)-1H-1,2,3-triazol-4-yl)methyl)-2-oxoindolin-3-ylidene)hydrazinecarboxamide (7f)

Yield 81%, light yellow solid, MP = 220–222 °C, IR (KBr, ν_{max}/cm^{-1}): 3469 (–NH); 3124 (C–H triazole); 1714 (C=O); 1697 (–N–C=O); 1681 (C=O); 1608 (–C=N), 3469 (–NH); 3124 (C–H triazole); 1714 (C=O); 1693 (–N–C=O); 1606 (C=O); 1575 (–C=N) ^{1}H NMR (400 MHz, DMSO-d_6) δ 5.12 (s, 2H, $–CH_2$); 6.44 (s, 2H, $–NH_2$ (exchangeable with D_2O)); 7.12 (d, $J = 8.6$ Hz, 1H, Ar–H); 7.41 (d, $J = 7.8$ Hz, 1H, Ar–H); 7.47–7.58 (m, 4H, 2Ar–H + $–NH_2$ (exchangeable with D_2O)); 7.71–8.03 (m, 2H, Ar–H + triazole-H); 8.27 (d, $J = 7.8$ Hz, 1H, Ar–H); 8.51 (s, 1H, –CH=N); 10.27 (s, 1H, –NH (exchangeable with D_2O)); 11.47 (s, 1H, –NH (exchangeable with D_2O)). ^{13}C NMR (100 MHz, DMSO-d_6) δ 35.1, 108.2, 112.7, 117.5, 121.3, 126.5, 126.8, 127.3, 130.2, 130.4, 130.7, 130.8, 134.5, 135.2, 135.7, 142.8, 155.3, 157.3, 157.8, 161.4. HRMS (ESI) calcd for $C_{20}H_{16}Br_2N_{10}O_3$ $[M(^{79}Br) + H]^+$ 602.9774 and $[M(^{81}Br) + H]^+$ 604.9753, found 602.9721 and 604.9640.

4.4 Molecular docking protocols

The molecular docking was performed using Schrodinger (Schrödinger Release 2022–1: Maestro, Schrödinger, LLC, New York, NY). Crystal co-ordinates of Ribonucleotide reductase (RNR) (PDB ID:2EUD) were downloaded from the protein data bank (www.rcsb.org). In the first step, bond orders were assigned and hydrogens were added by preprocess option. All water molecules were deleted. The heteroatoms are ionized by epic at biological pH to consider the protein permeability and drug solubility and then the H-Bonds were optimized to reduce the steric clashes by histidine, aspartate, glutamate, and hydroxyl containing amino acids. Then complete protein structure was minimized by using OPLS 2005 force field. Ligand preparation is generally required because molecules lack 3D coordinates, ionization, stereochemistry and tautomers. Thus, before docking, the least energy state of ligand was needed to be prepared. Ligprep tool of Schrödinger was used to prepare the least energy state of ligand which converts 1D/2D structures to 3D. Finally, this ligand molecule was minimized with the help of the OPLS 2005 force field. For docking, the grids were generated by using the grid-based energy descriptor which had a default set of options with Vander Waals radius of 1.0. The glide docking of the molecules was carried out using the previously prepared receptor grid and the ligand molecules.Thefavourable interactions between ligand molecules and the receptor were scored using Glide ligand docking program. All the docking calculations were performed using extra precision (XP) mode and OPLS-2005 force field. Thus H-Bonding, hydrophobic interactions and π–π stacking between enzyme and compound were determined [34–36].

4.5 Biological Evaluation

4.5.1 Cell Culturing

MCF-7 cells (ECACC) were cultured in Dulbecco's modified eagle's media (DMEM) and supplemented with 10% (foetal bovine serum) FBS and 1% penicillin–streptomycin. MDA-MB 231 cells (ATCC) were cultured in 3:1 DMEM with HAMS F12 media supplemented with 10% FBS and 1% penicillin–streptomycin, both incubated at 37 °C and 5% carbon dioxide (CO_2) to mimic in-vivo conditions.

4.5.2 MTT Assay

MCF-7 and MDA-MB 231 cells were seeded at a density of 5000 cells per well in triplicate into a 96-well plate and incubated 37 °C and 5% CO_2 for 24 h (hrs). Test compounds were dissolved in dimethylsulphoxide (DMSO) and working solutions were diluted in DMEM. Cells were treated with a range of different concentrations(1, 5, 10, 20, 50, 100 µM) of the various compounds for 24 h at 37 °C and 5% CO_2. Subsequently, sterile 5 µl of 5 mg/mL MTT (Sigma-Aldrich) dissolved in PBS was added to each well and incubated with cells for 2–3 h. Solubilisation solution (10% sodium dodecyl sulphate (SDS), 10 mM hydrochloric acid (HCl)) of equal volume to the wells was then added and incubated for 16 h at 37 °C. The optical density of each well was read at 570 nm using a microtiter plate reader (Thermo Fisher Scientific Multiskan GO Microplate Reader, SkanIt™ software) [37].

4.5.3 Statistical Analysis

The statistical analysis was performed using Excel® and IC_{50}values were estimated using GraphpadPrism5 software (Hearne Scientific Software). The experiments were performed in triplicates and at least two times for reproducibility. The statistical significance was calculated using student's *t*-test. A *p*-value of less than 0.05 was used to estimate the significance of the observations. A Z-factor was calculated

for each 96-well plate and assays having Z-factor above > 0.6 were included in the statistical analysis [38].

4.6 Spectroscopic and Electrochemical Measurements

Shimadzu 1601 spectrophotometer was used to record UV–Vis spectra of **6b** with or without addition of metal ions using quartz cuvette (path length, 1 cm). An electrochemical workstation (Autolab PGSTAT302N, Metrohm) was used to carry out electrochemical measurements i.e. Cyclic Voltammetry (CV) and Differential Pulse Voltammetry (DPV) using three electrode system consisting Glassy Carbon, Ag/AgCl and Pt wire as working, reference and counter electrodes, respectively. CV and DPV were carried out in the potential range from − 2.6 to − 1.0 V using 0.01 mol/L tetrabutylammonium perchlorate (TBAP) as supporting electrolyte and DMSO as solvent. Prior to each eletrochemical measurement, the contents were purged with high purity nitrogen gas to create an inert environment. All electrochemical measurements were performed at ambient temperature of 25.0 ± 1 °C.

Supplementary Information The online version contains supplementary material available at https://doi.org/10.1007/s42250-025-01274-4.

Declarations

Conflicts of Interest The authors declare no conflicts of interest.

References

1. https://cancerstatisticscenter.cancer.org/#/ (accessed on 27 Nov 2023).
2. Zheng G, Leone JP (2022) Male breast cancer: an updated review of epidemiology, clinicopathology, and treatment. J Oncol. https://doi.org/10.1155/2022/1734049
3. Feng Y, Spezia M, Huang S, Yuan C, Zeng Z, Zhang L, Ji X, Liu W, Huang B, Luo W, Liu B (2018) Breast cancer development and progression: risk factors, cancer stem cells, signaling pathways, genomics, and molecular pathogenesis. Genes Dis 5:77–106. https://doi.org/10.1016/j.gendis.2018.05.001
4. Golubnitschaja O, Debald M, Yeghiazaryan K, Kuhn W, Pešta M, Costigliola V, Grech G (2016) Breast cancer epidemic in the early twenty-first century: evaluation of risk factors, cumulative questionnaires and recommendations for preventive measures. Tumor Biol 37:12941–12957. https://doi.org/10.1007/s13277-016-5168-x
5. Rosenberg LU, Magnusson C, Lindström E, Wedrén S, Hall P, Dickman PW (2006) Menopausal hormone therapy and other breast cancer risk factors in relation to the risk of different histological subtypes of breast cancer: a case-control study. Breast Cancer Res 8:1–13. https://doi.org/10.1186/bcr1378
6. Arnold M, Morgan E, Rumgay H, Mafra A, Singh D, Laversanne M, Vignat J, Gralow JR, Cardoso F, Siesling S, Soerjomataram I (2022) Current and future burden of breast cancer: Global statistics for 2020 and 2040. Breast 66:15–23. https://doi.org/10.1016/j.breast.2022.08.010
7. Ahmad I (2018) Tamoxifen a pioneering drug: an update on the therapeutic potential of tamoxifen derivatives. Eur J Med Chem 143:515–531. https://doi.org/10.1016/j.ejmech.2017.11.056
8. Afrasiabi Z, Almudhafar R, Xiao D, Sinn E, Choudhury A, Ahmad A, Vyas A, Sarkar F, Padhye S (2013) Metal-based anticancer agents: targeting androgen-dependent and androgen-independent prostate and COX-positive pancreatic cancer cells by phenanthrenequinone semicarbazone and its metal complexes. Transit Met Chem 38:665–673. https://doi.org/10.1007/s11243-013-9735-3
9. Knox JJ, Hotte SJ, Kollmannsberger C, Winquist E, Fisher B, Eisenhauer EA (2007) Phase II study of Triapine® in patients with metastatic renal cell carcinoma: a trial of the National Cancer Institute of Canada Clinical Trials Group (NCIC IND. 161). Invest New Drugs 25:471–477. https://doi.org/10.1007/s10637-007-9044-9
10. Traynor AM, Lee JW, Bayer GK, Tate JM, Thomas SP, Mazurczak M, Graham DL, Kolesar JM, Schiller JH (2010) A phase II trial of Triapine® (NSC# 663249) and gemcitabine as second-line treatment of advanced non-small cell lung cancer: Eastern Cooperative Oncology Group Study 1503. Invest New Drugs 28:91–97. https://doi.org/10.1007/s10637-009-9230-z
11. Lindemann A, Patel AA, Silver NL, Tang L, Liu Z, Wang L, Tanaka N, Rao X, Takahashi H, Maduka NK, Zhao M (2019) COTI-2, a novel thiosemicarbazone derivative, exhibits antitumor activity in HNSCC through p53-dependent and -independent mechanisms. Clin Cancer Res 25:5650–5662. https://doi.org/10.1158/1078-0432.ccr-19-0096
12. Pape FS, Enyedy É, Keppler B, Kowol CR (2019) Anticancer thiosemicarbazones: chemical properties, interaction with iron metabolism, and resistance development. Antioxid Redox Signal 30:1062–1082. https://doi.org/10.1089/ars.2017.7487
13. Jia X, Liu Q, Wang S, Zeng B, Du G, Zhang C, Li Y (2020) Synthesis, cytotoxicity, and in vivo antitumor activity study of parthenolide semicarbazones and thiosemicarbazones. Bioorg Med Chem 28:115557. https://doi.org/10.1016/j.bmc.2020.115557
14. Ali SM, Azad MA, Jesmin M, Ahsan S, Rahman MM, Khanam JA, Islam MN, Shahriar SM (2012) In vivo anticancer activity of vanillin semicarbazone. Asian Pac J Trop Biomed 2:438–442. https://doi.org/10.1016/S2221-1691(12)60072-0
15. Chauhan G, Pathak DP, Ali F, Dubey P, Khasimbi S (2022) In-vitro evaluation of isatin derivatives as potent anti-breast cancer agents against MCF-7, MDA-MB-231, MDA-MB-435, and MDA-MB-468 breast cancer cell lines: a review. Anticancer Agents Med Chem 22:1883–1896. https://doi.org/10.2174/1871520621666210903130152
16. Hoff PM, Wolff RA, Bogaard K, Waldrum S, Abbruzzese JL (2006) A phase I study of escalating doses of the tyrosine kinase inhibitor semaxanib (SU5416) in combination with irinotecan in patients with advanced colorectal carcinoma. Jpn J Clin Oncol 36:100–103. https://doi.org/10.1093/jjco/hyi229
17. Haddad JJ (2022) The immunopharmacologic potential of Semaxanib and new generation directed therapeutic drugs: receptor tyrosine kinase regulation with anti-tumorigenesis/angiogenesis properties. Saudi Pharm J 20:103–123. https://doi.org/10.1016/j.jsps.2011.09.002
18. Abdel-Aziz HA, Eldehna WM, Keeton AB, Piazza GA, Kadi AA, Attwa MW, Abdelhameed AS, Attia MI (2017) Isatin-benzoazine molecular hybrids as potential antiproliferative agents: synthesis and in vitro pharmacological profiling. Drug Des Dev Ther 11:2333–2346. https://doi.org/10.2147/dddt.s140164
19. Chowdhary S, Shalini AA, Kumar V (2022) A mini review on isatin, an anticancer scaffold with potential activities against

neglected tropical diseases (NTDs). Pharmaceuticals 15(5):536. https://doi.org/10.3390/ph15050536
20. Mushtaq A, Asif R, Humayun WA, Naseer MM (2024) Novel isatin–triazole based thiosemicarbazones as potential anticancer agents: synthesis, DFT and molecular docking studies. RSC Adv 14(20):14051–14067. https://doi.org/10.1039/D4RA01234J
21. Mehreen S, Ullah A, Nadeem H, Dege N, Naseer MM (2022) Synthesis, solid-state self-assembly driven by antiparallel π···π stacking and {/HCCF}(2) dimer synthons, and in vitro acetylcholinesterase inhibition activity of phenoxy pendant isatins. RSC Adv 12(3):1788–1796. https://doi.org/10.1039/D1RA08286H
22. Abbasi I, Nadeem H, Saeed A, Kharl HAA, Tahir MN, Naseer MM (2021) Isatin-hydrazide conjugates as potent α-amylase and α-glucosidase inhibitors: synthesis, structure and in vitro evaluations. Bioorg Chem 116:105385. https://doi.org/10.1016/j.bioorg.2021.105385
23. Khatoon S, Aroosh A, Islam A, Kalsoom S, Ahmad F, Hameed S, Abbasi SW, Yasinzai M, Naseer MM (2021) Novel coumarin-isatin hybrids as potent antileishmanial agents: synthesis, in silico and in vitro evaluations. Bioorg Chem 110:104816. https://doi.org/10.1016/j.bioorg.2021.104816
24. Sharma B, Singh A, Gu L, Saha ST, Singh-Pillay A, Cele N, Singh P, Kaur M, Kumar V (2019) Diastereoselective approach to rationally design tetrahydro-β-carboline–isatin conjugates as potential SERMs against breast cancer. RSC Adv 9:9809–9819. https://doi.org/10.1039/c9ra00744j
25. Chowdhary S, Raza A, Preeti KS, Anand A, Sharma AK, Kumar V (2023) Isatin-indoloquinoxaline click adducts with a potential to overcome platinum-based drug-resistance in ovarian cancer. Bioorg Chem 142:106953. https://doi.org/10.1016/j.bioorg.2023.106953
26. Preeti RA, Anand A, Henry N, Sharma AK, Roussel P, Kumar V (2023) Stereo/regio-selective access to substituted 3-hydroxyoxindoles with anti-proliferative assessment and in silico validation. RSC Adv 13:28434–28443. https://doi.org/10.1039/d3ra05869g
27. Sharma B, Kumar S, Preeti JMD, Kremer L, Kumar V (2022) 1H–1,2,3-triazole embedded isatin-benzaldehyde-bis (heteronuclearhydrazones): Design, synthesis, antimycobacterial, and cytotoxic evaluation. Chem Biol Drug Des 99:301–307. https://doi.org/10.1111/cbdd.13984
28. Myers JM, Cheng Q, Antholine WE, Kalyanaraman B, Filipovska A, Arnér ES, Myers CR (2013) Redox activation of Fe(III)–thiosemicarbazones and Fe(III)–bleomycin by thioredoxin reductase: specificity of enzymatic redox centers and analysis of reactive species formation by ESR spin trapping. Free Radic Biol Med 60:183–194. https://doi.org/10.1016/j.freeradbiomed.2013.02.016
29. Popović-Bijelić A, Kowol CR, Lind ME, Luo J, Himo F, Enyedy EA, Arion VB, Gräslund A (2011) Ribonucleotide reductase inhibition by metal complexes of Triapine (3-aminopyridine-2-carboxaldehyde thiosemicarbazone): a combined experimental and theoretical study. J Inorg Biochem 105:1422–1431. https://doi.org/10.1016/j.jinorgbio.2011.07.003
30. Martinie RJ, Blaesi EJ, Krebs C Jr, Bollinger JM, Silakov A, Pollock CJ (2017) Evidence for a di-μ-oxo diamond core in the Mn(IV)/Fe(IV) activation intermediate of ribonucleotide reductase from *Chlamydia trachomatis*. J Am Chem Soc 139:1950–1957. https://doi.org/10.1021/jacs.6b11563
31. Taher AT, Khalil NA, Ahmed EM (2011) Synthesis of novel isatin-thiazoline and isatin-benzimidazole conjugates as anti-breast cancer agents. Arch Pharm Res 34:1615–1621. https://doi.org/10.1007/s12272-011-1005-3
32. Pontarin G, Ferraro P, Bee L, Reichard P, Bianchi V (2012) Mammalian ribonucleotide reductase subunit p53R2 is required for mitochondrial DNA replication and DNA repair in quiescent cells. Proc Natl Acad Sci U S A 109:13302–13307. https://doi.org/10.1073/pnas.1211289109
33. Brignole EJ, Tsai KL, Chittuluru J, Li H, Aye Y, Penczek PA, Stubbe J, Drennan CL, Asturias F (2018) 3.3-Å resolution cryo-EM structure of human ribonucleotide reductase with substrate and allosteric regulators bound. eLife 7:e31502. https://doi.org/10.7554/eLife.31502
34. Greenwood JR, Calkins D, Sullivan AP, Shelley JC (2010) Towards the comprehensive, rapid, and accurate prediction of the favorable tautomeric states of drug-like molecules in aqueous solution. J Comput Aided Mol Des 24:591–604. https://doi.org/10.1007/s10822-010-9349-1
35. Shivakumar D, Williams J, Wu Y, Damm W, Shelley J, Sherman W (2010) Prediction of absolute solvation free energies using molecular dynamics free energy perturbation and the OPLS force field. J Chem Theory Comput 6:1509–1519. https://doi.org/10.1021/ct900587b
36. Jorgensen WL, Maxwell DS, Tirado-Rives J (1996) Development and testing of the OPLS all-atom force field on conformational energetics and properties of organic liquids. J Am Chem Soc 118:11225–11236. https://doi.org/10.1021/ja9621760
37. Sagar S, Esau L, Moosa B, Khashab NM, Bajic VB, Kaur M (2014) Cytotoxicity and apoptosis induced by a plumbagin derivative in estrogen-positive MCF-7 breast cancer cells. Anticancer Agents Med Chem 14:170–180. https://doi.org/10.2174/1871520611313660369
38. Zhang JH, Chung TD, Oldenburg KR (1999) A simple statistical parameter for use in evaluation and validation of high throughput screening assays. J Biomol Screen 4:67–73. https://doi.org/10.1177/108705719900400206